High-Resolution Raman and Luminescence Spectroscopy of Isotope-Pure (SiC)-Si-28-C-12, Natural and C-13 - Enriched 4H-SIC

Ivan Gueorguiev Ivanov, Milan Yazdanfar, Björn Lundqvist, Jr-Tai Chen, Jawad ul-Hassan, Pontus Stenberg, Rickard Liljedahl, Nguyen Tien Son, Joel W. III Ager, Olle Kordina and Erik Janzén

Original Publication:

Ivan Gueorguiev Ivanov, Milan Yazdanfar, Björn Lundqvist, Jr-Tai Chen, Jawad ul-Hassan, Pontus Stenberg, Rickard Liljedahl, Nguyen Tien Son, Joel W. III Ager, Olle Kordina and Erik Janzén, High-Resolution Raman and Luminescence Spectroscopy of Isotope-Pure (SiC)-Si-28-C-12, Natural and C-13 - Enriched 4H-SIC, 2014, Silicon Carbide and Related Materials 2013, PTS 1 AND 2, (), , 471-474.
http://dx.doi.org/10.4028/www.scientific.net/MSF.778-780.471

High-Resolution Raman and Luminescence Spectroscopy of Isotope-Pure $^{28}Si^{12}C$, Natural and ^{13}C – Enriched 4H-SiC

Ivan G. Ivanov[1,a *], Milan Yazdanfar[1], Björn Lundqvist[1], Jr-Tai Chen[1], Jawad Hassan[1], Pontus Stenberg[1], Rickard Liljedahl[1], Nguyen T. Son[1], Joel W. Ager III [2], Olof Kordina[1] and Erik Janzén[1]

[1] Department of Physics, Chemistry and Biology, Linköping University, 581 83 Linköping, Sweden

[2] Lawrence Berkeley National Laboratory, Berkeley, California 94720, USA

[a]ivani@ifm.liu.se

Keywords: isotope-pure SiC, isotope-enriched SiC, Raman spectroscopy, photoluminescence, bandgap variation with isotope content

Abstract. The optical properties of isotope-pure $^{28}Si^{12}C$, natural SiC and enriched with ^{13}C isotope samples of the 4H polytype are studied by means of Raman and photoluminescence spectroscopies. The phonon energies of the Raman active phonons at the Γ point and the phonons at the M point of the Brillouin zone are experimentally determined. The excitonic bandgaps of the samples are accurately derived using tunable laser excitation and the phonon energies obtained from the photoluminescence spectra. Qualitative comparison with previously reported results on isotope-controlled Si is presented.

Introduction

Replacement of natural SiC with isotope-pure silicon carbide composed exclusively of ^{12}C and ^{28}Si is expected to improve the performance of this material in several applications. The improved thermal conductivity (presumably, up to 30%) will boost the performance of electronic and optoelectronic components and make them more economic due to reduced need of cooling. A number of other known applications will also benefit from the isotope purity, e.g., shielding of nuclear fuel particles with pure $^{28}Si^{12}C$ is expected to solve the problem with conversion of ^{30}Si to P during nuclear reactions, which eventually leads to cracking the shield. Also, isotope-pure $^{12}C^{28}Si$ has obvious advantage for spintronics applications owing to the absence of nuclear spins in the crystal matrix. It has been shown recently as well that isotope-pure graphene has by ~20% larger thermal conductivity (at 300 K) than its counterpart containing carbon in its natural abundance [1], and similar anticipation can be made for graphene grown by sublimation on $^{28}Si^{12}C$. Recent measurements on 4H-$^{28}Si^{12}C$ have estimated at least 18% improvement of the thermal conductivity at room temperature compared to natural 4H-SiC [2]. This study is concerned with comparative investigation of the optical properties of natural and isotope-controlled samples of 4H-SiC, including accurate determination of the phonon energies and the excitonic bandgap.

Experimental Details

The investigated 4H-SiC samples include isotope-purified $^{28}Si^{12}C$ samples [with isotope purity 99.85% for ^{28}Si and 99.98% for ^{12}C as determined by secondary ion mass spectrometry (SIMS)], ^{13}C-enriched sample (~50% ^{13}C as determined by SIMS), and a reference sample with natural isotope abundance (^{nat}SiC with 98.9% ^{12}C and 1.1% ^{13}C, and 92.2% ^{28}Si, 4.7% ^{29}Si, and 3.1% ^{30}Si). Most of the optical measurements are performed in a double monochromator (SPEX 1404) coupled to photomultiplier with maximum resolution of 0.05 Å (about 42 μeV in the near-bandgap region of 4H-SiC) using tunable laser excitation. Micro-Raman measurements are also employed for accurate determination of the relative shifts of the Raman peaks depending on the isotope composition. The substrate was removed from the investigated samples, however, polishing-induced stress lead to broadening of the no-phonon lines in the low-temperature photoluminescence spectrum. Hence,

another $^{28}Si^{12}C$ sample with the substrate on was used for measurements of the linewidth of the nitrogen-bound exciton no-phonon lines. However, no polishing-induced broadening could be observed in the Raman lines.

Results and Discussion

Raman spectra. All Raman measurements are performed in backscattering geometry. However, different configurations with respect to the crystal axis (c-axis) of the 4H-SiC samples were used in order to obtain information of all phonon modes allowed in Raman scattering. Using the labeling of the phonons according to the irreducible representation of the point group C_{6v}, the Raman-active phonons are $3A_1 + 3E_1 + 4E_2$ (the $3A_1 + 3E_1$ modes are also active in infrared absorption). Thus, a total of ten lines are expected in the Raman spectrum, but not all of them appear if a single experimental geometry is used. In addition, the splittings in the folded transversal acoustic modes have never been observed and a total of eight lines appear in the Raman spectra of 4H-SiC [3].

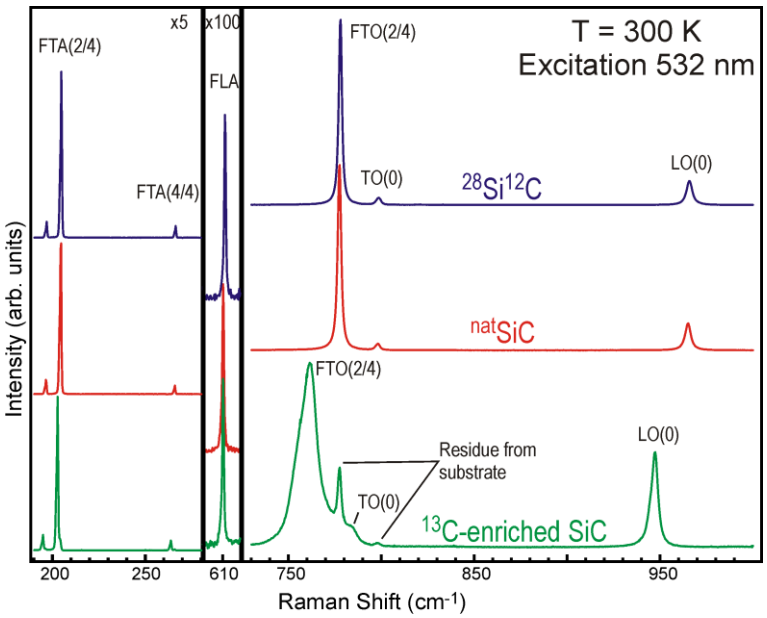

Fig. 1. Raman spectra of the three investigated samples in near-backscattering along the crystal c-axis geometry. Note the horizontal axes breaks and the scale changes.

Typical Raman spectra in the conventional backscattering from the surface geometry demonstrating the peak shifts for the different samples are presented in Fig. 1. The absolute peak positions are summarized in Table 1. We notice that although the error in determination of the peak positions is ± 0.2 cm^{-1}, this error is systematic across all data rather than random. Hence, the peak shifts with respect to the isotope-pure $^{28}Si^{12}C$ have much better accuracy, probably below 0.05 cm^{-1} (except for the broader LO and TO modes in the ^{13}C-enriched sample). These shifts and the line broadening (the line widths are also displayed in Table 1) are due to differences in the isotope composition, as discussed below.

The stiffest modes (highest Raman shifts) for all the lines are observed in the $^{28}Si^{12}C$ sample, as expected in view of the "lightening" of the atomic weight of both atomic species and the intuitive anticipation that the squared vibrational frequency would scale as the inverse of the atomic mass. Useful approximation used to describe the effect of mass disorder due to presence of different isotopes in any of the C or Si sublattices is the virtual crystal approximation (VCA) [4], although much more accurate theory exists for elemental crystals, e.g., diamond [5]. Hereafter we use the notations of [3,4] for the folded modes (e.g., FLA(x) for longitudinal and FTA(x) for transversal acoustic modes, respectively, with x=0, 2/4 or 4/4 for 4H-SiC, etc.). The frequencies of the TO(0) and LO(0) modes in the notations of [3,4] in the ^{13}C-enriched should scale according to VCA as the inverse square root of the reduced mass, $M_r = \bar{M}_C^{-1} + \bar{M}_{Si}^{-1}$, where $\bar{M}_C = 12 + x/100$ and $\bar{M}_{Si} = 28 + y_1/100 + 2y_2/100$ are the average masses (in amu) for C and Si in SiC containing x% ^{13}C, y_1% ^{29}Si, and y_2% ^{30}Si. Using as a reference the energies of TO(0) and LO(0) in $^{28}Si^{12}C$, the calculated frequencies for the other two samples are given in Table 1. Another mode, FLA(1), appearing around 610 cm^{-1} in 4H-SiC has the special property that the displacements of the C atoms nearly vanish for this mode [6,7]. This explains the same (within the experimental accuracy) position of this mode in the Raman spectra of the ^{nat}SiC and ^{13}C-enriched SiC (610.2 cm^{-1}), since both samples have the same natural abundance of Si isotopes. Hence the VCA can be applied but with different

mass factor for scaling the $^{28}Si^{12}C$-energy, namely, the ratio $\sqrt{M_{Si}/\bar{M}_{Si}}$ involving Si masses only, where M_{Si}= 28 amu is the ^{28}Si isotope mass. In most cases VCA produces only rough estimation of the experimental phonon energies, similar to the case of diamond [5].

Table 1. Raman shifts [cm^{-1}] for the investigated samples. The linewidths (FWHM) of the TO modes are shown below each mode. The calculated theoretical phonon energies are results of the VCA calculation and are given in parentheses after the experimental ones with a subscript T (where applicable, as explained in text).

Phonon	FTA(2/4)	FTA(4/4)	FLA(4/4)	FTO(2/4)	TO(0)	LO(0)
$^{28}Si^{12}C$	196.4, 204.6	265.6	611.1	777.2	798.2	965.1
	FWHM < 0.8	< 0.8	< 0.8	FWHM 2.2	FWHM 2.3	FWHM ~3.6
^{nat}SiC	196.0, 204.25	265.05	610.2(609.9_T)	776.7(776.5_T)	797.9(797.5_T)	964.2(964.2_T)
	FWHM < 0.8	< 0.8	< 0.8	FWHM 2.3	FWHM 2.4	FWHM ~3.6
^{13}C-enriched	194.4, 202.7	262.8	610.2(609.9_T)	~756(765.8_T)	~784(786.5_T)	~945(950.9_T)
	FWHM < 0.8	< 0.8	< 0.8	FWHM >13	FWHM 6.3	FWHM ~4.6

The observed linewidths of the Raman lines also deserve attention. While the optical modes exhibit significant broadening in the ^{nat}SiC and especially the ^{13}C-enriched samples compared to the $^{28}Si^{12}C$ sample, no broadening could be detected for the folded acoustic modes (FLA, FTA). The latter are very narrow, with linewidths below 0.25 cm^{-1} in ^{nat}SiC [3]. The main mechanism of line broadening is elastic scattering of the phonons induced by mass defects [4]; according to the theory [8] the magnitude of the broadening $\Delta\Gamma$ of a mode with frequency ω is proportional to $\Delta\Gamma \sim \omega^2 g |\mathbf{e}|^4 \rho(\omega)$, where $\rho(\omega)$ is the phonon density of states, **e** is the relevant phonon eigenvector and g is the relative mass variance. In the case of FLA and FTA modes the weight of the Si eigenvector dominates in **e** and the relative mass variance is much smaller for Si than for C. In addition, the factor ω^2 contributes another order of magnitude in diminishing $\Delta\Gamma$ for the low-energy modes in comparison to the optical modes, which explains why the isotope-induced broadening is not observed with our experimental resolution (about 0.8 cm^{-1}).

The optical modes are fitted with convolution of Lorentzian and triangular line shapes with the linewidth of the latter fixed at the spectrometer resolution (0.8 cm^{-1}). The resulting widths of the Lorentzians are listed in Table 1 and are in overall agreement with the semi-empirical theoretical curves of Ref. [4] (cf. Fig. 3 of this reference).

Photoluminescence (PL) and excitonic bandgap determination. The low-temperature PL spectra of the three investigated samples are compared in Fig. 2. High-resolution measurement reveals that the linewidth of the nitrogen bound exciton (NBE) no-phonon line (Q_0) of the $^{28}Si^{12}C$ sample is smaller (possibly, much smaller) than the maximum achievable spectral resolution in our system (0.05 Å, or ~45 μeV, see the insert of Fig. 2), while the corresponding line is significantly broader in the other two samples. The phonon replicas of the shallower NBE line P_0 and the free exciton replicas are clearly visible in the spectra. Two observations are worth mentioning before proceeding with the excitonic-bandgap determination. We notice a shift of the NBE lines with the isotope composition (cf. Fig. 2), but the softening of the phonon modes with increasing content of heavier isotopes is much smaller than for the Raman modes. We use the energies of two phonons determined from the PL spectra to calculate the excitonic bandgap E_{gx}. One of them is the lowest-energy phonon in $^{28}Si^{12}C$, ^{nat}SiC and ^{13}C-enriched SiC, with energy E_{33} of 33.15 ± 0.05, 33.10 ± 0.05, and 32.90 ± 0.05 meV, respectively. The rise of the phonon-assisted absorption in each of the samples will occur at $E_{gx} + E_{ph}$. We use tunable laser excitation and scan it across and above the absorption edge. The luminescence is recorded in the region of the strongest *free-exciton* (FE) replica (cf. Fig. 2); the energy of the phonon responsible for this replica is 76.45 ± 0.05, 76.40 ± 0.05, and 76.25 ± 0.05 meV in $^{28}Si^{12}C$, ^{nat}SiC and ^{13}C-enriched samples, respectively. When the excitation energy is within ~1 meV above the absorption edge the sharp peek due to hot free-exciton recombination, H_{76} [9], is visible, too, and allows accurate determination of E_{gx}. We obtain

the values 3265.8 ± 0.1, 3266.0 ± 0.1, and 3268.1 ± 0.1 meV for the excitonic bandgaps of $^{28}Si^{12}C$, ^{nat}SiC, and ^{13}C-enriched samples, respectively. The decrease of the bandgap with increasing content of heavier isotopes is in qualitative agreement with results obtained with isotope-controlled silicon, indicating that also in silicon carbide the electron-phonon interaction seems to be the dominant mechanism for the observed renormalization of the bandgap [10]. We notice that the shift of the excitonic bandgap accounts for most of the shift observed for the NBE lines and the phonon replicas in the spectra.

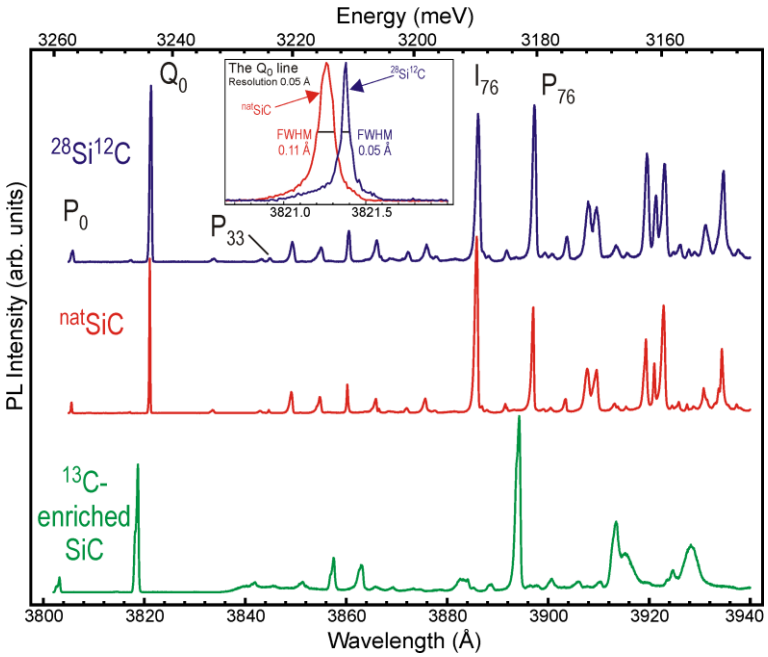

Fig. 2. Low-temperature PL spectra of the samples excited with above-bandgap laser energy. The insert compares the linewidth of another isotope-pure (with the substrate on) and the reference samples.

Summary

We present a comparative study of the optical properties of isotope-pure $^{28}Si^{12}C$ and samples with other isotope compositions. The shifts and the broadening of the Raman lines with increasing isotope disorder are clearly observed, as well as the shift of the phonons at the M-point of the Brillouin zone of 4H-SiC, as observed in the PL spectra. The excitonic bandgaps of the investigated samples are accurately determined. The observed increase in the bandgap with increasing isotope disorder is in qualitative agreement with the results for silicon and accounts for (most of) the shift of the NBE no-phonon lines.

Acknowledgements. Support from the Swedish Research Council, the Swedish Foundation for Strategic Research, and the Knut and Alice Wallenberg Foundation is gratefully acknowledged.

References

[1] S. Chen, Q. Wu, C. Mishra, J. Kang, H. Zhang, K. Cho, W. Cai, A.A. Balandin and R.S. Ruoff, Nature Mat. 11 (2012) 203.

[2] B. Lundqvist *et al.*, presented at 19th International Workshop on Thermal Investigations of ICs and Systems (September 25-27, 2013, Berlin, Germany).

[3] S. Nakashima and H. Harima, phys. stat. sol. (a) 162 (1997) 39.

[4] S. Rohmfeld, M. Hundhausen, L. Ley, N. Schulze and G. Pensl, Phys. Rev. Lett. 86(2001) 826.

[5] K.C. Hass, M.A. Tamor, T.R. Anthony and W.F. Banholzer, Phys. Rev. B 45 (1992) 7171.

[6] F. Widulle, T. Ruf, O. Buresch, A. Debernardi, M. Cardona, Phys. Rev. Lett. 82 (1999) 3089.

[7] K. Karch, P. Pavone, W. Windl, O. Schütt and D. Strauch, Phys. Rev. B 50 (1994) 17054.

[8] S. Tamura, Phys. Rev. B 30, 849 (1984).

[9] I.G. Ivanov, T. Egilsson, A. Henry, B. Monemar and E. Janzén, Phys. Rev. B 64(2001) 085203.

[10] S. Tsoi, H. Alawadhi, X. Lu, J.W. Ager III, C.Y. Liao, H. Riemann, E.E. Haller, S. Rodriguez and A.K. Ramdas, Phys. Rev. B 70 (2004) 193201.